APPROXIMATE METHODS FOR THERMOVISCOELASTIC CHARACTERIZATION AND ANALYSIS OF ELASTOMERIC LEAD-LAG DAMPERS

G.Hausmann, P.Gergely
EUROCOPTER Deutschland
Munich,Germany

Abstract

An engineering method for the nonlinear thermoviscoelastic characterization of elastomeric dampers in the frequency domain was developed and numerically realized .
Material equations are represented in terms of amplitude dependent complex moduli.Effects of material nonlinearities, heat buildup and environmental conditions on the damper efficiency were studied by a thermoviscoelastic model with concentrated parameters.This model describes the steady state and transient thermal behaviour including special cases such as low temperature stiffening and thermal runaway.An application of this thermomechanical model for the prediction of rotor blade damping is demonstrated.In addition a short outline is given to a damper model with distributed parameters.

1. Introduction

Elastomeric lead-lag dampers are widely used in modern soft-inplane bearingless rotor systems as the primary source for damping.
An optimum damper design has to take into account the operational variables including temperature extremes and service life deterioration without serious loss of damping / 10,12,13 /.
Due to the high thermal sensitivity of the physicomechanical properties and the low heat conduction of elastomers the influence of dissipative heating, environmental temperature and air cooling on damper performance and durability is of significant importance in damper design.
For this reason, investigations of the intensity of internal heat generation in relation to thermomechanical material properties, loading amplitude, frequency and heat release capacity are of considerable practical interest.
The present paper describes an approximate theory of the thermoviscoelastic behaviour of elastomeric dampers , reflecting experiences gained during the development of the bearingless BO 108 (EC155) - rotor system (see Figure 1).

Presented at the 18th European Rotorcraft Forum, 15-18 September 1992, Avignon, France

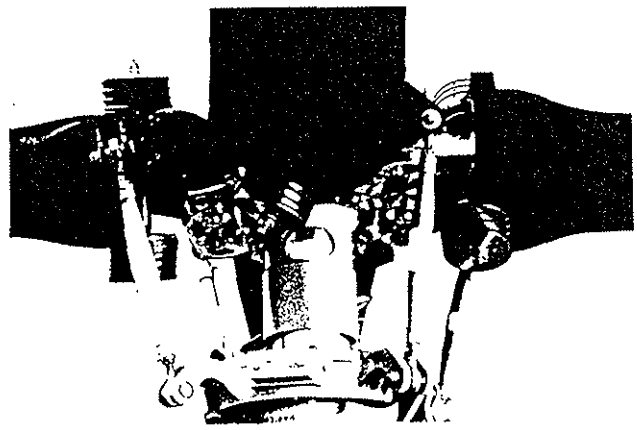

Fig.1: The BO108 main rotor system

2. Thermomechanical Damper Model with Concentrated Parameters

Stiffness and dissipation energy are global,directly measurable properties of elastomeric dampers.
The analytical characterization of dampers by means of these integral quantities leads to concentrated parameter models.
This formulation is consistent with the principle of energy conservation and based on a homogeneous distribution of strains and temperature.
In the frequency domain the equations for spring rates and dissipation energy are represented in terms of amplitude and temperature dependent complex moduli.This engineering approach yields a useful analytical tool for predicting the thermoviscoelastic response at different loads and environmental conditions.In the following,the investigations are limited to a representative damper model under cyclic shear.Superposition of dissipation energy rates allows an approximate generalization of this method to simultaneous multiaxial cyclic loads.

2.1 Thermoviscoelastic Characterization in the Frequency Domain

2.1.1 Experimental Determination of Mechanical Properties

For the characterization of the nonlinear visco - elastic behaviour of elastomeric dampers two kinds of experiments are usually conducted /4,13,14/ :

Short time tests
Dynamic tests with mono (poly-) harmonic displacement (force-) controlled loads at different combinations of amplitudes, frequencies and temperature.

Long-term tests
Relaxation (creep-) tests at different load amplitudes and temperatures.

In the first case, the load, displacement and temperature are recorded continuously and numerically analyzed for the determination of the complex springrate and hysteresis area.
In the second case, load (resp. displacement) and temperature are recorded continuously. The numerical analysis yields the relaxation (creep-) function and the static equilibrium modulus dependent on amplitude and temperature.
A sketch of a typical test setup for dynamic shear tests is shown in Figure 2.

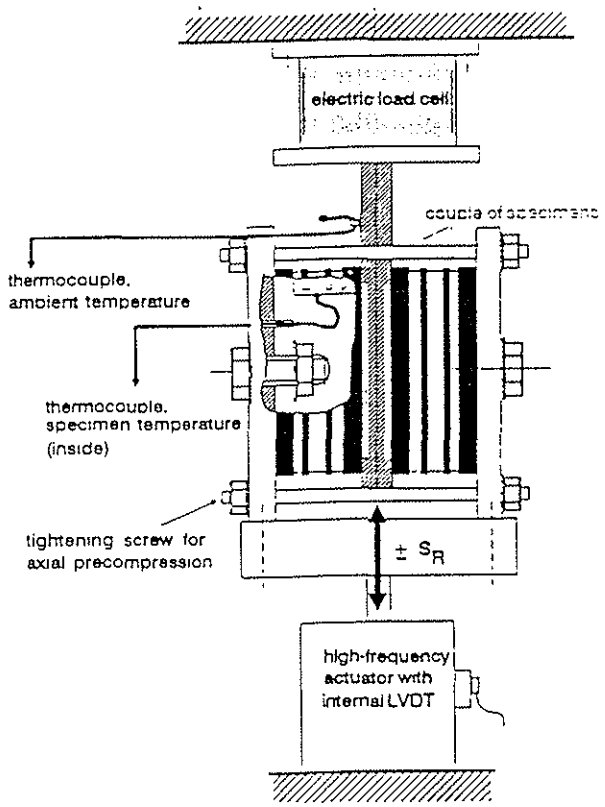

Fig.2 : Test setup for dynamic shear tests.

2.1.2 Idealization of Measured Hysteresis Loops

Measured monofrequent hysteresis loops show in the nonlinear range a more or less significant deviation from the ideal viscoelastic elliptic shape. For the analytical characterization of real damper properties (based on the methods of the classic theory of viscoelasticity),such nonlinear hysteresis loops are appropriately idealized by means of the following two equivalent criteria

- same values of loop area (dissipation energy per cycle W_{Diss})
- same values of the amplitude of force F and displacement x

The dynamic spring rate |K*| and the mechanical loss factor $\eta = \tan\delta$ in the two types of loops are identical (method of equivalent damping energy). This widely used method leads to the introduction of an amplitude dependent complex modulus in the sense of generalization of the linear theory of viscoelasticity / 5 ,9,15,18 /. This allows an adequate simulation of the damper characteristic in respect to complex stiffness, loss factor and dissipation energy (heat build up).
Figure 3 shows this "linearization" procedure in form of a sketch.

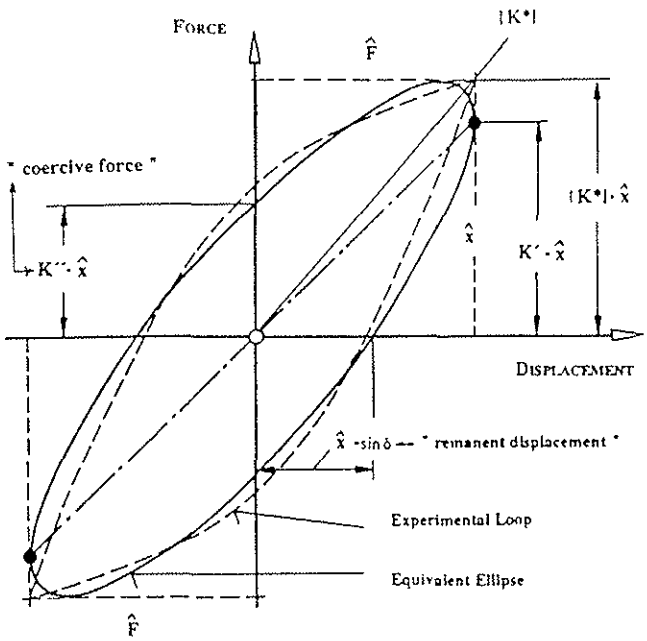

Fig.3 : Quasi - linearization of a measured hysteresis loop (principle sketch) .

Complex stiffness |K*| and mechanical loss factor $\eta = \tan\delta$ are defined in this context as

$$|K^*| = F / x$$

$$\eta = \tan\left[\arcsin\left(\frac{W_{Diss}}{\pi \cdot F \cdot x}\right)\right]$$

2.1.3 Nonlinear Analytical Characterization

2.1.3.1 Factorization of Complex Viscoelastic Quantities

A widely reported and experimental verified method / 5,13,15,18/ for the characterization of nonlinear thermoviscoelastic material properties in the frequency domain is based on the definition of amplitude and temperature dependent complex moduli .
The generalization of the classical theory of viscoelasticity to mechanical nonlinearity and thermomechanical coupling yields the following interrelations between force- and displacement controlled loading conditions in the frequency domain.

- Displacement-controlled viscoelastic response:

$$F(x,\omega,\vartheta,t,...) = |K^*(x,\omega,\vartheta,t,...)|\ x$$

$$K^*(x,\omega,\vartheta,t,...) = K'(x,\omega,\vartheta,t,...) + i\ K''(x,\omega,\vartheta,t,...)$$

$$\eta\ (x,\omega,\vartheta,t,...) = K''(x,\omega,\vartheta,t,...)/K'(x,\omega,\vartheta,t,...)$$

- Force-controlled viscoelastic response:

$$x\ (F,\omega,\vartheta,t,...) = |J^*\ (F,\omega,\vartheta,t,...)|\ F$$

$$J^*\ (F,\omega,\vartheta,t,...) = J'\ (F,\omega,\vartheta,t,...) - i\ J''\ (F,\omega,\vartheta,t,...)$$

$$\eta\ (F,\omega,\vartheta,t,...) = J''\ (F,\omega,\vartheta,t,...)/J'\ (F,\omega,\vartheta,t,...)$$

Complex springrate K* and complex compliance J* are connected here by the following relations

$$J'^{(\prime)}\ (F,\omega,\vartheta,t,...) = K'^{(\prime)}(x,\omega,\vartheta,t,...)\ /\ |K^*(x,\omega,\vartheta,t,...)|^2$$

$$|J^*(F,\omega,\vartheta,t,...)| = |K^*(x,\omega,\vartheta,t,...)|^{-1}$$

and

$$\eta(F,\omega,\vartheta,t,...) = \eta\ (x,\omega,\vartheta,t,...)$$

with

$$F = |K^*(x,\omega,\vartheta,t,...)|\ x$$

From the theoretical point of view,both descriptions of the complex moduli are equivalent.
In order to characterize adequately these visco - elastic quantities, it is advantageous to introduce explicit analytical expressions.
Experimental investigations show that effects of mechanical (amplitude) and thermal nonlinearity can be approximated by separable functions within the working range of the lead-lag damper /13 ,15 /.
The difference between measured values and the approximation by separable functions of amplitude and temperature effects is comparatively small and can be accepted in this engineering approach.

With the definition of a parameter range and an appropriate selection of a reference point P (P (x_p, ω_p, ϑ_p, t_p, ...)) within this "working window" the following factorization with regard to amplitude, frequency and temperature is obtained :

$$K'(x,\omega,\vartheta) = K'_p\ g'(x)\ h'(\omega,\vartheta)$$

$$K''(x,\omega,\vartheta) = K''_p\ g''(x)\ h''(\omega,\vartheta)$$

$$\eta(x,\omega,\vartheta) = \eta_p\ g_\eta(x)\ h_\eta(\omega,\vartheta)\ ,$$

with:

$$g'^{(\prime\prime)}(x_p) = 1\ ,\ h'^{(\prime\prime)}(\omega_p,\vartheta_p) = 1,$$

$$g_\eta\ (x_p) = 1\ ,\ h_\eta\ (\omega_p,\vartheta_p) = 1,$$

in the working point P.
In addition to an adequate theoretical character - ization of the damper performance, this approxi - mation allows a significant reduction of component tests by analytical inter- /extrapolation of test results within the corresponding working range.
The determination of the nondimensional corre - lation functions "g" resp. "h" is part of the next chapters.

2.1.3.2 Effect of Amplitude

The viscoelastic response of high damping elastomers shows a strong nonlinear dependence of the loading amplitude.
For example, the effect of different shear ampli - tudes x on damper characteristics (hysteresis loops) is presented in Figure 4 for a widely used type of silicon rubber.

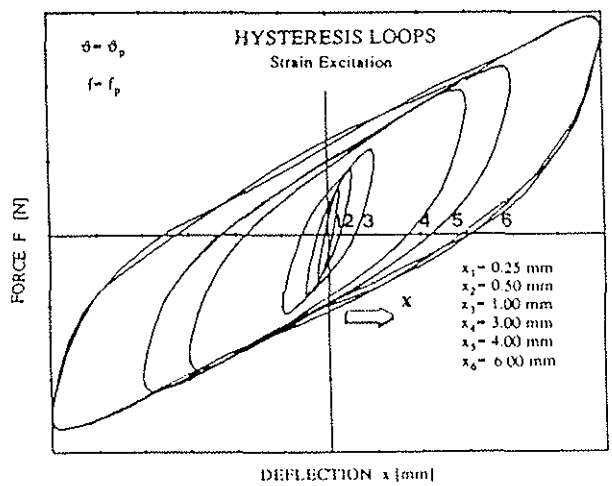

Fig. 4 : Effect of amplitudes on damper characteristic

The analysis of component tests shows for each viscoelastic quantity K', K", K* and η another amplitude dependency. Due to the interdepen - dency of the complex viscoelastic functions, only two functions (e.g. K' and η) are sufficient for the complete analytical characterization.
The nondimensional amplitude function for K' is defined as

$$g'(x) = K'(x, \omega_p, \vartheta_p)/K'_p \ .$$

A good analytical approximation of the experi - mental results is given by the following fit-function

$$g'(x) = C_1 + (C_2 - C_1) / (\exp A) \quad , \text{ where}$$

$$A = (\ln(1 + |x/x_0|)/C_3)^{C_4}$$

with

x_0 = 1mm and $C_1, \ldots, C_4$ = fit parameters.

The parameters C_1 to C_4 are determined by means of a nonlinear regression analysis according to the Levenberg-Marquardt method / 8 /. Another approach is the use of nonlinear optimizing tools, see for example Ref. / 19 /.

The corresponding amplitude function of the mechanical loss factor was found as

$$g_\eta(x) = \eta(x, \omega_p, \vartheta_p)/\eta_p = C_1 + C_2(1 - e^{-A}) - C_4(1 - e^{-B})$$

with $A = C_3 |x/x_0|$ and $B = C_5 |x/x_0|$.

Figure 5 shows the characteristic shape of such nonlinearity dimensionless functions.

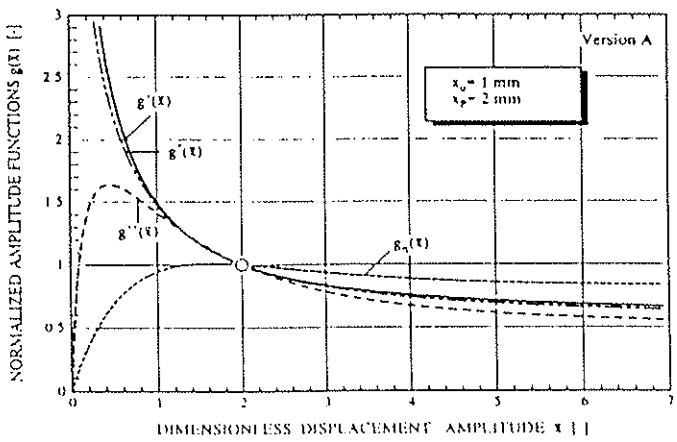

Fig. 5 : Dimensionless amplitude functions

The correlation with the remaining two amplitude functions g'(x) resp. g"(x) is given to

$$g''(x) = g'(x)\, g_\eta(x) \qquad \text{and}$$

$$g^*(x) = 1/K_p^* \left((K_p' \, g'(x))^2 + (K_p'' \, g''(x))^2 \right)^{1/2} \ .$$

Figure 6 to 7 show measured and analytically fitted springrates and loss factors in dependency of displacement amplitudes .

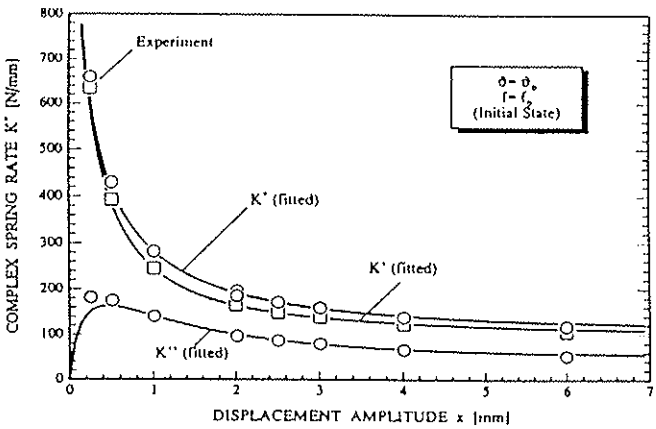

Fig. 6 : Complex stiffness as a function of displacement amplitude

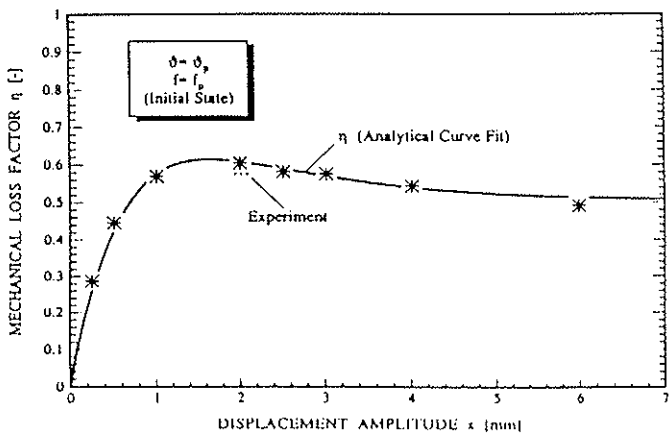

Fig. 7 : Mechanical loss factor as a function of displacement amplitude

The corresponding diagram for the complex compliance J* as a function of the force amplitude is given in Fig. 8 .
In addition,Fig. 9 shows the mechanical loss factor η in dependency of the force amplitude.
The analytical relationships between cyclic strain and stress excitations are given in chapter 2.1.3.1 .

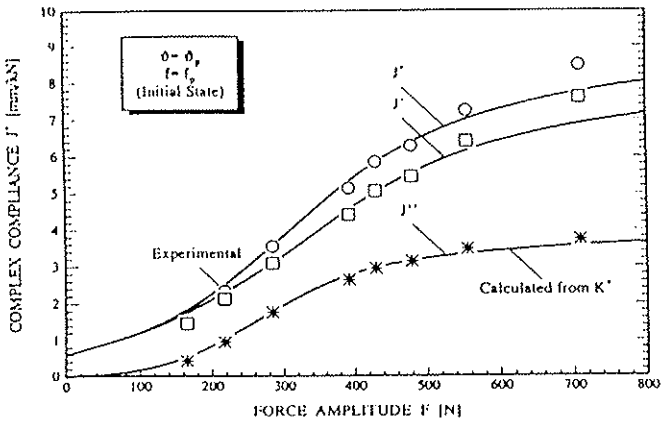

Fig. 8 : Complex compliance versus force amplitude

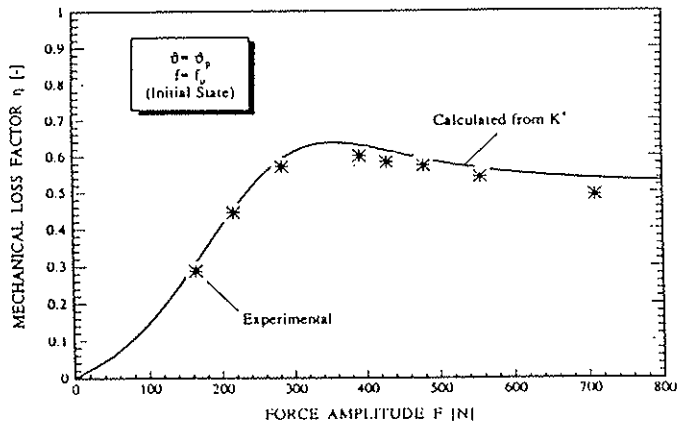

Fig. 9 : Mechanical loss factor versus force amplitude

2.1.3.3 Effect of Frequency

An example of the effect of frequency on the damper characteristic is shown in Figure 10. The dimensionless frequency functions can be approximated within a limited frequency range by the following empirical equations.

$$h'(\omega) = h'(\omega,\vartheta_p) = K'(x_p,\omega,\vartheta_p)/K'_p$$

$$= C_1 + C_2(\omega/\omega_0)^{C_3}$$

$$h_\eta(\omega) = h_\eta(\omega,\vartheta_p) = \eta(x_p,\omega,\vartheta_p)/\eta_p$$

$$= C_4(\omega/\omega_0)^{C_5}$$

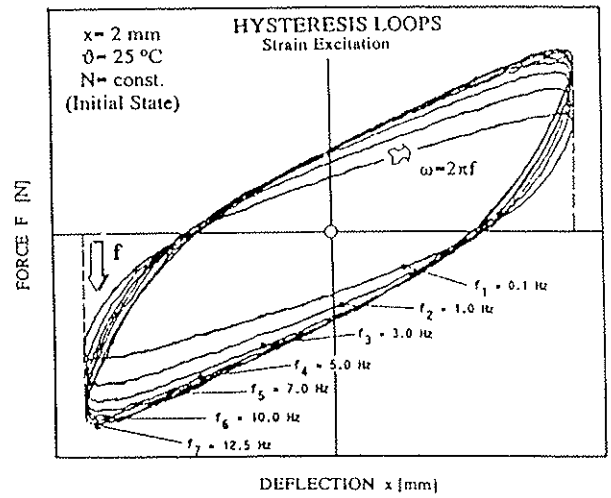

Fig. 10 : Damper characteristic as a function of frequency

The other two frequency functions h" and h* can be derived from the relations

$$h''(\omega) = h''(\omega,\vartheta_p) = h'(\omega)\, h_\eta(\omega)$$

and

$$h^*(\omega) = 1/K_p^* \left((K_p' h'(\omega))^2 + (K_p'' h''(\omega))^2 \right)^{1/2}$$

Figure 11 shows these isothermal frequency functions for a selected damper material.

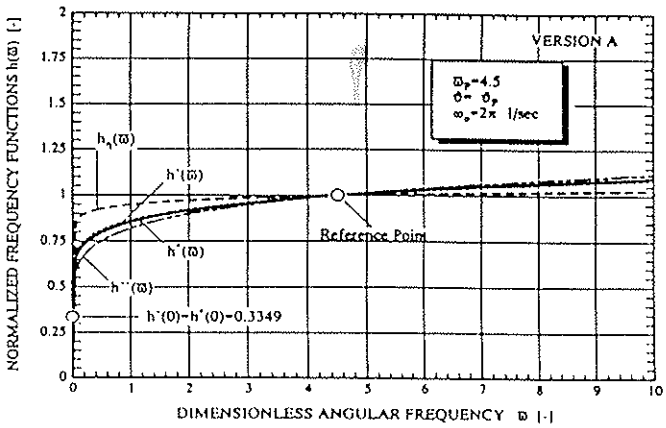

Fig. 11 : Normalized isothermal frequency functions

2.1.3.4 Effect of Temperature

Silicon rubber has a very low glass transition temperature and shows the slightest temperature

dependence of all elastomers with respect to stiffness and damping. Nevertheless, temperature is an important parameter and has a decisive influence on stiffness and dissipation characteristic. For example,the effect of different ambient temperatures on damper characteristic is shown in Fig.12.

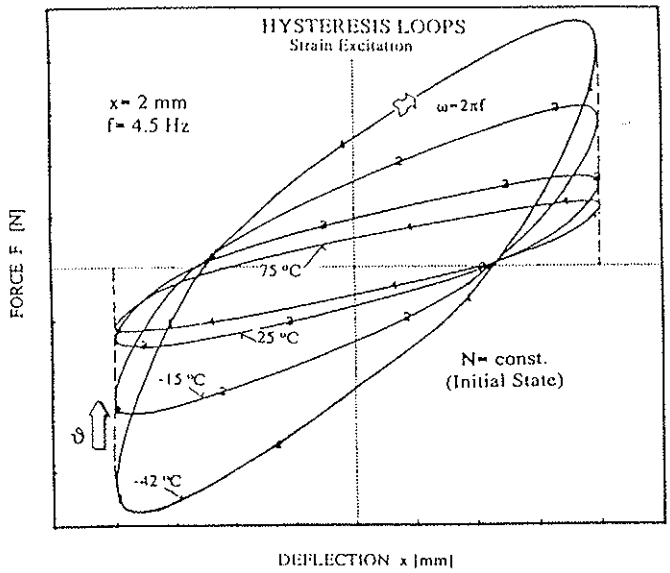

Fig 12 : Damper characteristic as a function of ambient temperature

The corresponding test setup is shown in Fig. 13.

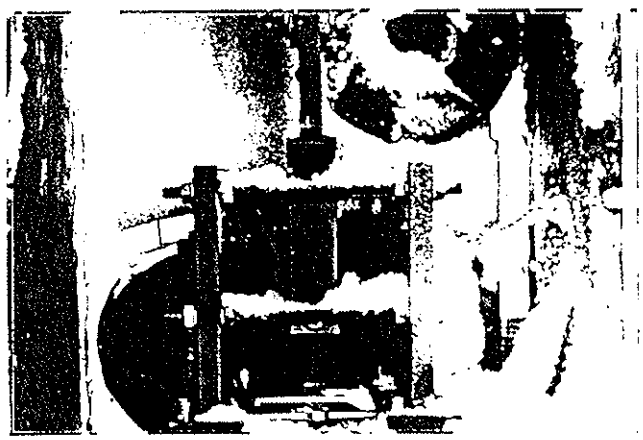

Fig . 13 : Test setup for cold start simulation (laboratory conditions)

Due to the low thermal conductivity and a significant dependency of the mechanical characteristics on temperature, dissipative heating is of considerable influence on damper perform'- ance. As an example, Figures 14 and 15 show the effect of self - heating on damper characteristic dependent on loading time resp. load cycles. The effect of cool stream is neglectable in the initial phase, but its velocity has a significant influence on the thermal equilibrium state.

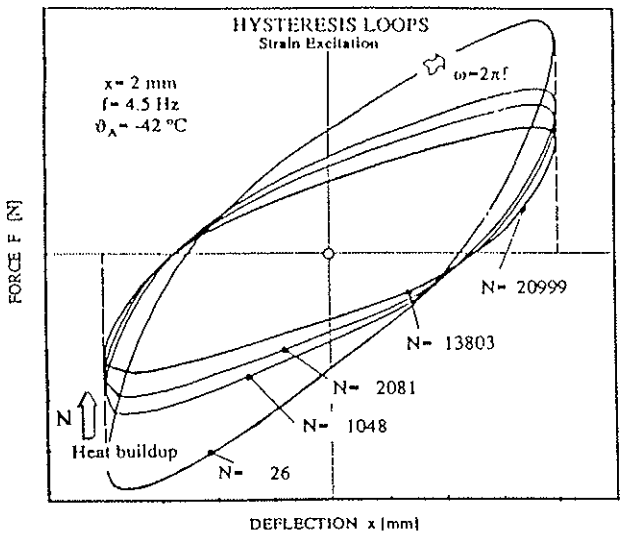

Fig . 14 : Hysteresis loop as a function of warm-up time (laboratory conditions)

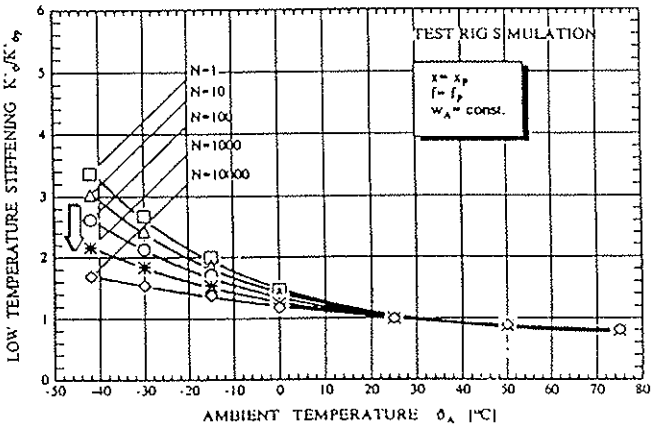

Fig. 15 : Low temperature stiffening (laboratory conditions)

Experimental investigations /3/ show a thermo - rheologically complex material behaviour /5,16 / , where the effect of temperature can be characte- rized by two different nonlinear shift-functions $a_T(\vartheta)$ and $b_T(\vartheta)$.These shift-functions are introduced as follows

$$K'^{(*)}(x_p,\omega,\vartheta) = b_T(\vartheta)\ K_p'^{(*)}\ h'^{(*)}(\omega\ a_T(\vartheta))$$

$$|K^*(x_p,\omega,\vartheta)| = b_T(\vartheta)\ K^*_p\ h^*(\omega\ a_T(\vartheta))$$

$$\eta(x_p,\omega,\vartheta) = \eta_p\ h_\eta(\omega\ a_T(\vartheta))$$

with $\omega = \omega/\omega_0$ and

$$a_T(\vartheta_p) = b_T(\vartheta_p) = 1.$$

The frequency-temperature coupling of the horizontal shift function $a_T(\vartheta)$ permits no further decomposition (factorization) of these influence parameters.
The temperature function $a_T(\vartheta)$ is adequately approximated by the expression

$$a_T(\vartheta) = 10^R \quad ; \quad R = \sum_{i=1}^{N} a_i (1 - (T/T_p)^{b_i}$$

with $T = 273 + \vartheta$ and $T_p = 298\ K$.

An approach for $b_T(\vartheta)$ is given by

$$b_T(\vartheta) = \sum_{j=0}^{M} c_j (\vartheta - \vartheta_p)^j$$

Figure 16 shows these shift-functions (N = 2 resp. M = 4) for a high damping silicon rubber.

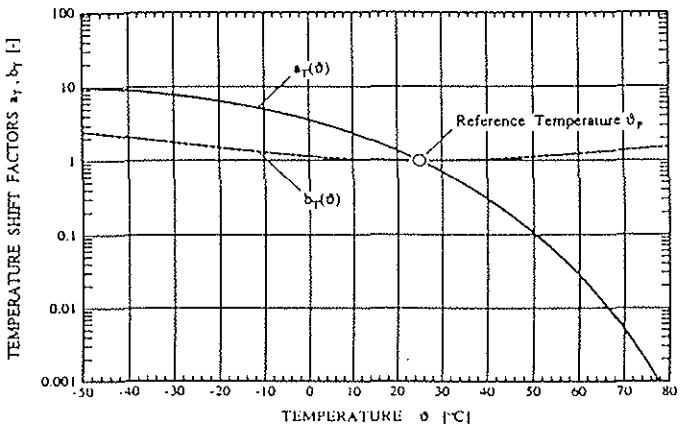

Fig.16 : Temperature shift - functions $a_T(\vartheta)$ and $b_T(\vartheta)$

The corresponding approximation of stiffness and loss factor is presented in Figures 17 and 18 .

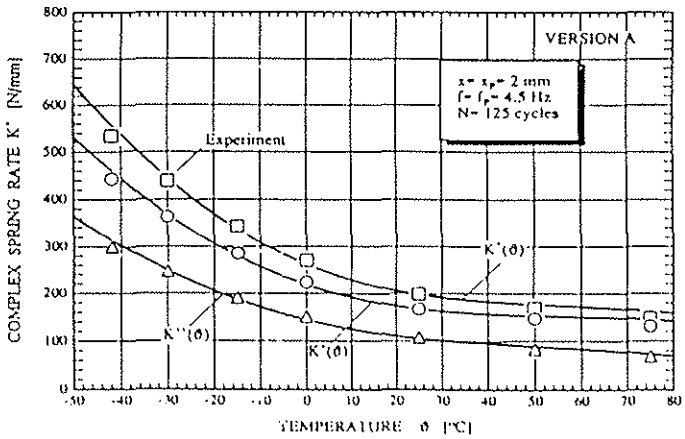

Fig.17 : Temperature effect on spring rates

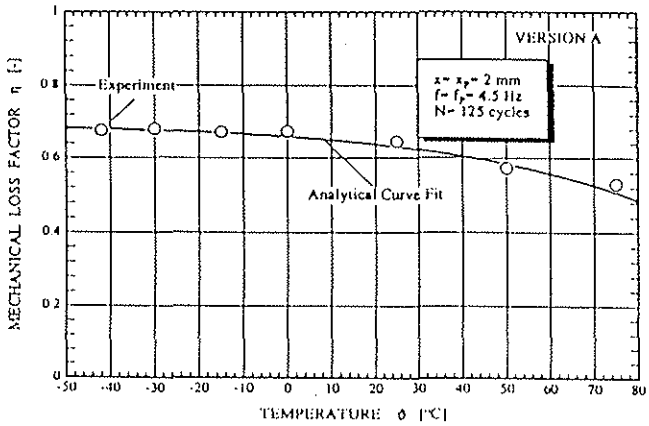

Fig.18 : Temperature effect on mechanical loss factor

2.2 Dissipation Function for Cyclic Shear Deformation

2.2.1 Basic Theory

For thermomechanical problems with cyclic deformations it is often convenient to consider the mean rate of energy dissipation rather than the detail of the temperature history over a cycle of deformation /11/.
The mean or "cycle-averaged" dissipation rate can be calculated as :

$$\overline{\dot{Q}}_+ = \frac{\omega}{2\pi} \int_t^{t+\frac{2\pi}{\omega}} \dot{Q}(t')dt' = \frac{\omega}{2\pi} \int_t^{t+\frac{2\pi}{\omega}} F(t')\,\dot{x}(t')dt' = N_{Diss}$$

with $\omega = 2\pi f$.

The definition of the cycle - averaged temperature history is shown in Figure 19.

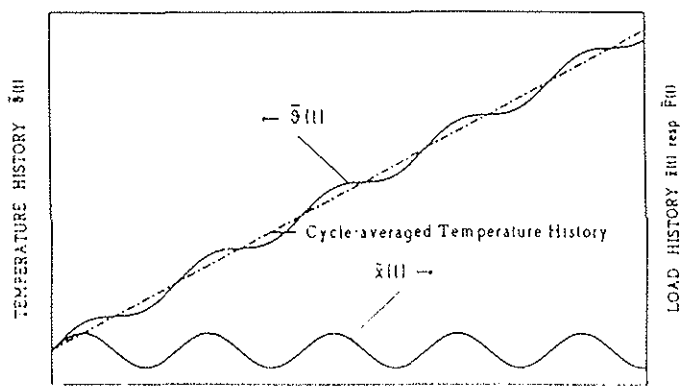

Fig. 19 : Temperature and load histories at cyclic excitation

2.2.2 Monoharmonic displacement-controlled loading

In the case of displacement-controlled loading (strain excitation), the cycle-averaged dissipation rate has the general form /5,17 /:

$$\overline{\dot{Q}}_+ = N_{Diss} = f\ W_{Diss} = \frac{\omega}{2} K''(x,\omega,\vartheta)\ x^2$$

The analytical approximation by separable functions becomes

$$N_{Diss} = \frac{\omega}{2} K''_p\ g''(x)\ h''(\omega a_T(\vartheta))\ b_T(\vartheta)\ x^2$$

Figure 20a to 20b show this high nonlinear dissipation function in dependency of amplitude, frequency and temperature.

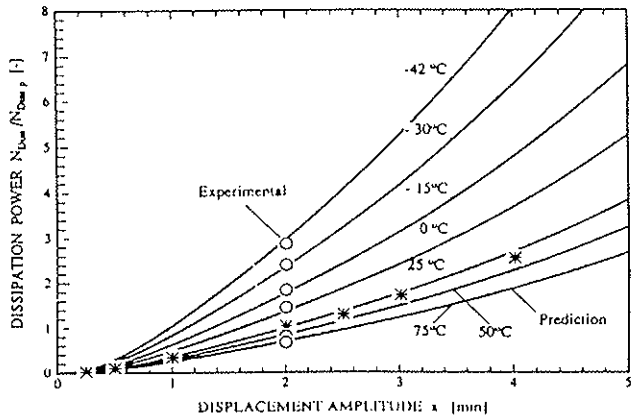

Fig. 20 a

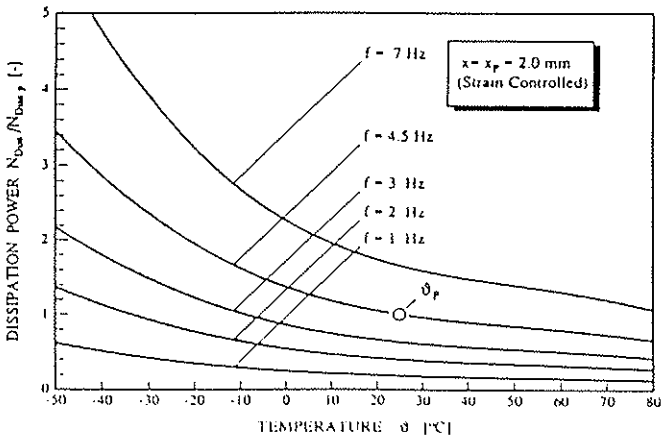

Fig. 20 b

Fig. 20 : Dissipation rate as a function of dis - placement amplitude,frequency and temperature.

2.2.3 Monoharmonic force-controlled loading

For force-controlled monoharmonic loads the mean energy dissipation rate becomes

$$\overline{\dot{Q}}_+ = N_{Diss} = f\ W_{Diss} = \frac{\omega}{2} J''(F,\omega,\vartheta)\ F^2$$

with J" as imaginary part of the complex compliance.
The interconversion of the viscoelastic quantities J* and K* is given in chapter 2.1.3.1 .
Figure 21 shows the average dissipation rate as a function of force amplitude and temperature.

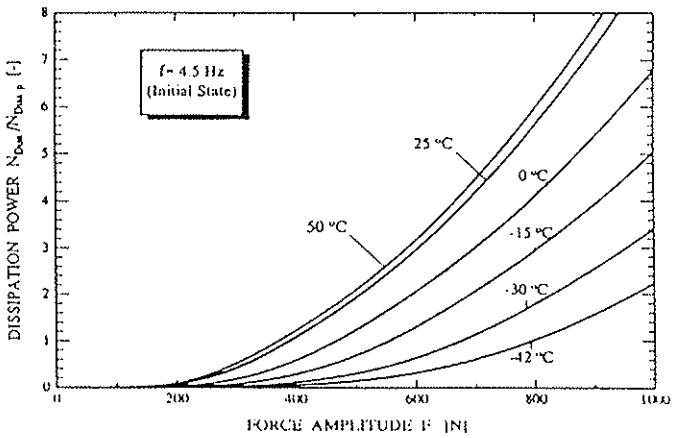

Fig. 21 : Dissipation energy as a function of force amplitude and temperature.

2.2.4 Polyharmonic Loading

The measured nonlinear viscoelastic response to a superposed harmonic displacement function

$$x(t) = x_1 \sin \omega_1 t + x_2 \sin \omega_2 t$$

with x_1 = 4 mm, x_2 = 2 mm and f_1 = 7 Hz , f_2 = 4 Hz is presented in Figure 22 for the thermal state of equilibrium .
The measured history of dissipation energy over a cycle of deformation is shown in Figure 23 .
A comparison of the cycle-averaged dissipation energies for the corresponding monofrequent and bifrequent load cases is given in Table 1.

	Measured energies		Corrigated (isothermal) energies	
	$\overline{\dot{Q}}(\vartheta)$	$\Delta\vartheta_E$ *)	$\overline{\dot{Q}}(\vartheta_{ref})$	$\vartheta_{E,ref}$ *)
$x_1(t)$	30.3 W	16.2 °C	29.4 W	46.1 °C
$x_2(t)$	6.9 W	2.2 °C	4.3 W	46.1 °C
x (t)	32.8 W	21.1 °C	32.8 W	46.1 °C

*) $\Delta\vartheta_E$: difference between initial temperature and thermal equilibrium temperature
$\vartheta_{E,ref}$: reference temperature for isothermal energy correction

Table 1 : Dissipation energies at multiharmonic loading

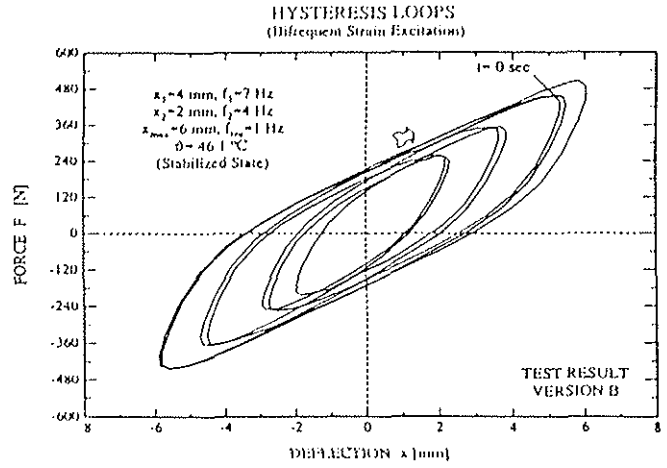

Fig. 22 : Multiharmonic viscoelastic response (strain excitation)

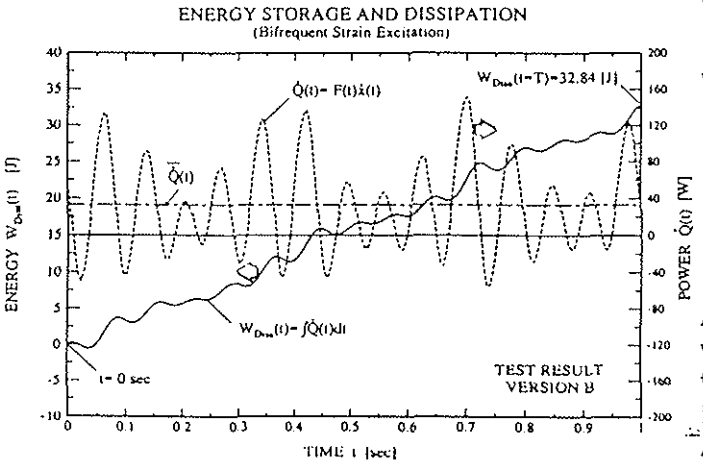

Fig. 23 : Energy histories at polyharmonic loading

The linear theory of viscoelasticity leads to a superposition principle for the cycle-averaged dissipation rates at isothermal conditions.
The deviations in Table 1 from this principle are founded in nonlinearities due to amplitude effects, temperature differences and long-term hereditary effects.
The validity of this superposition principle for dissipation powers is assumed here for nonlinear - viscoelastic materials at isothermal conditions, neglecting effects of amplitude dependency.
The mean dissipation rate for superposed force- (resp. deflection-) controlled cyclic loads is therefore given to

$$N_{Diss}(\vartheta) = \sum_i N_{Diss,i}(\vartheta)$$

or in terms of dissipation energies

$$W_{Diss} = \frac{1}{T} \sum f_i \, W_{Diss,i} \quad .$$

The validity of an isothermal superposition - principle is subject of further investigations (multi-frequency response of lead-lag dampers /12/).

An accurate, more advanced method for the calculation of energy rates at arbitrary load histories yields the direct numerical solution of the nonlinear-viscoelastic constitutive equation in the time domain (Volterra integral equation of the second kind, / 4,5/).

2.3 Heat Transmission

The cooling capacity is an important design para - meter for elastomeric dampers.
Assuming that the heat transmission is caused by convection, the rate of heat flow is described by the equation

$$\dot{Q}_- = \sum_i \alpha_i A_i \, \Delta\vartheta_i$$

where

α_i = heat transfer coefficients
A_i = surface areas
$\Delta\vartheta_i = \vartheta_i - \vartheta_A$ = temperature differences between surfaces and ambient temperature

A simplified heat transfer model was assumed here with a constant average temperature throughout the volume of the discrete damper model and over its surface.
An engineering approach for the global heat trans - mission can be found therefore by the following definition of an equivalent overall heat transfer coefficient α :

$$\dot{Q}_- = \alpha(\vartheta_A, v_A) \, A \, (\vartheta - \vartheta_A) = B(\vartheta_A, v_A) \, (\vartheta - \vartheta_A)$$

with $\alpha(\vartheta_A, v_A) = (1/A) \sum_i \alpha_i(\vartheta_A, v_A) \, A_i$ and $A = \sum_i A_i$

where ϑ = mean temperature of damper.

Appropriate formulae and data for the heat transfer at forced and free convection are given for example in references / 1 , 2 / .
Fig. 24 shows the overall heat transfer coefficient α for the considered damper as a function of the ambient temperature ϑ_A and the mean air velocity v_A .

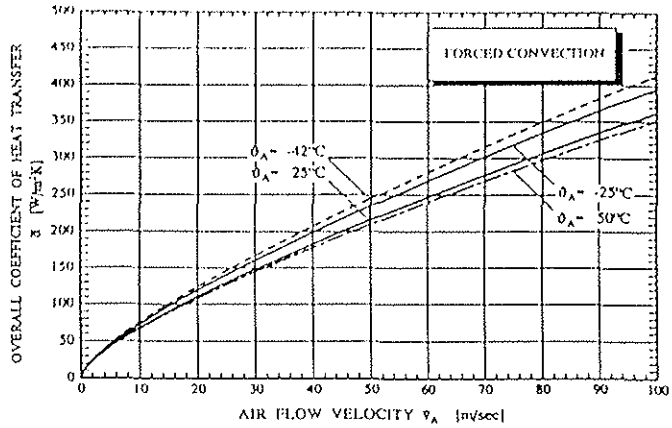

Fig. 24 : Overall coefficient of heat transfer versus air flow velocity and ambient temperature

The overall heat transfer (cooling) capacity at forced convection is therefore calculated as

$$B(\vartheta_A, v_A) = \alpha(\vartheta_A, v_A)\, A \ .$$

Effects of heat conduction and free convection are taken into account by addition of an equivalent heat transfer coefficient to α.

2.4 Coupled Energy Equation

2.4.1 Basic Considerations

The extent of the temperature rise depends on the heat capacity of the damper and on the balance between the rate of mechanical energy dissipation and the rate of heat loss to the surroundings. The temperature may reach a steady-state value if the rates of these two processes - heat generation (N_{Diss}) and heat loss ($\dot{Q}_-$)-become equal or it may increase indefinitely ("thermal runaway").
This thermomechanical process is shown schema - tically in Figures 25a to 25b .

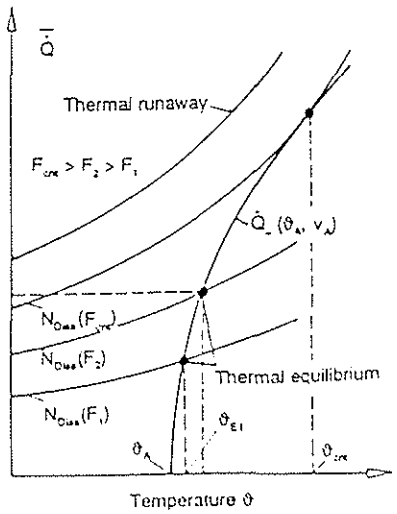

Fig. 25 a

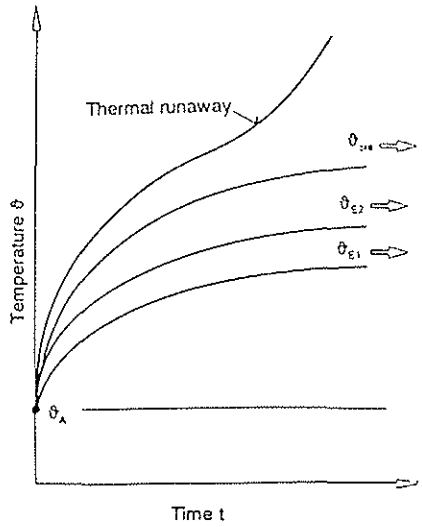

Fig. 25 b

Fig. 25 : Thermal equilibrium and thermal failure

2.4.2 Energy Balance

The global energy balance of the discrete damper model is given to

$$\dot{Q}_s = \overline{\dot{Q}_+} - \dot{Q}_- = N_{Diss} - \dot{Q}_-$$

with $\overline{\dot{Q}_+}$: Rate of heat generation
$\dot{Q}_-$: Outflow of heat
$\dot{Q}_s$: Rate of heat accumulation.
Thermal equilibrium exists if $\overline{\dot{Q}_+} = \dot{Q}_-$.
The rate of heat accumulation in the damper can be written as

$$\dot{Q}_s = C\ \dot{\vartheta}$$

where the heat storage capacity C of the damper is defined to

$$C = \sum_i c_i\, m_i = \sum_i c_i\, \rho_i\, V_i$$

with c : Specific thermal capacity
m : Mass
ρ : Density
V : Volume.

The summation (i) is carried out for the different parts of the damper, i.e. elastomer, shims and housings. The effect of temperature on specific thermal capacity and density was neglected here.

2.4.3 Differential Equations for the Damper Temperature

The energy balance yields the general differential equation for the (averaged) damper temperature $\vartheta = \overline{\vartheta}$:

$$C \frac{d}{dt}\vartheta(t) = \bar{\dot{Q}}_+(t) - B(\vartheta_A, v_A)\,(\vartheta(t) - \vartheta_A) \quad , \vartheta(0) = \vartheta_o .$$

This nonlinear differential equation is the basic formula for the following considerations.

2.4.3.1 Displacement-Controlled Cyclic Excitation

The explicit formulation of the energy term $\bar{\dot{Q}}_+(t)$ leads to the following nonlinear differential equation for the transient damper temperature

$$\frac{d}{dt}\vartheta = 1/C \left\{\frac{\omega}{2} K''_p\, g''(x)\, h''(\omega a_T(\vartheta))\, b_T(\vartheta)\, x^2 - B(\vartheta_A, v_A)(\vartheta - \vartheta_A)\right\}$$

The numerical solution by means of Runge-Kutta techniques ,/8/ ,requires the analytical characterization of the energy terms.
In the thermal steady state case ($d\vartheta/dt = 0$) this differential equation reduces to a nonlinear algebraic equation with respect to ϑ.
The numerical solution of this equation yields the equilibrium temperature ϑ_E of the damper .
No solution for ϑ_E exists in the case of thermal runaway ($\bar{\dot{Q}}_+ > \dot{Q}_-$).

The variation of damper stiffness and dissipation energy is coupled directly with the temperature history.

2.4.3.2 Force-Controlled Cyclic Excitation

For this case the temperature differential equation becomes:

$$\frac{d}{dt}\vartheta = 1/C \left\{\frac{\omega}{2} J''(F,\omega,\vartheta)\, F^2 - B(\vartheta_A, v_A)\,(\vartheta - \vartheta_A)\right\}$$

If the imaginary part of the complex compliance J" is not explicit known from force-controlled experiments, it can be substituted by K" as follows:

$$J''(x,\omega,\vartheta) = \frac{K''(x,\omega,\vartheta)}{K^*(x,\omega,\vartheta)^2} = \frac{\eta(x,\omega,\vartheta)}{1+\eta^2(x,\omega,\vartheta)}\ (1/\,K'(x,\omega,\vartheta)\,)$$

The relationship between force amplitude F and deflection amplitude x is generally given to

$$F - |K^*(x,\omega,\vartheta)|\ x = 0 .$$

Solving this nonlinear algebraic equation with regard to x (for a given F) yields the identity

$$J''\,(x(F),\omega,\vartheta) = J''(F,\omega,\vartheta).$$

2.4.3.3 Polyharmonic Excitation

The assumption of a superposition principle for the mean dissipation rates

$$\bar{\dot{Q}}_+ = \sum_i \dot{Q}_{+,i}$$

yields with the following expressions for the dissipation energies

$$\bar{\dot{Q}}_{+,i} = \frac{\omega_i}{2} K''(x_i,\omega_i,\vartheta)\, x^2 \quad \text{(displacement controlled)}$$

respectively

$$\bar{\dot{Q}}_{+,i} = \frac{\omega_i}{2} J''(F_i,\omega_i,\vartheta)\, F^2 \quad \text{(force controlled)} \ ,$$

the differential equation of damper temperature in a similar form as in the case of monoharmonic loading.
The equilibrium temperature is given again as solution of the equation

$$\bar{\dot{Q}}_+ - \dot{Q}_- = 0 .$$

2.4.3.4 Cooling Characteristic

The rate of cooling in the unloaded position is described by the solution of the differential equation

$$\frac{d}{dt}\vartheta(t) + (B(\vartheta_A, v_A)/C)(\vartheta - \vartheta_A) = 0 \quad \text{with } \vartheta(t_o) = \vartheta_o .$$

This equation is useful in the experimental identification of the relationship B/C .

2.5 Numerical Simulation of Thermomechanical Damper Characteristic

Based on the presented theory a numerical model was developed for the simulation of the thermo - mechanical damper characteristic.Examples of application of this model to realistic damper configurations are summarized in the following chapter. Figure 26 shows the thermal states of equilibrium at strain controlled loading conditions as intersection of the two curves N_{Diss} resp. $\dot{Q}_-$.
Stiffness,loss factor and therefore dissipation power decreases here with increasing heat build up. The case of stress controlled loading conditions is shown in Figure 27. Stiffness and loss factor decrease here also with selfheating, but higher deflections result in an increase of dissipation power.
This diagrams show,that thermal runaway is excluded for this damper configuration,but at high

load amplitudes -coupled with low cooling capacity- overheating of the damper can occur.
In both cases there is a significant influence of air velocity (and ambient temperature) on the damper equilibrium temperature and therefore on the damper performance.

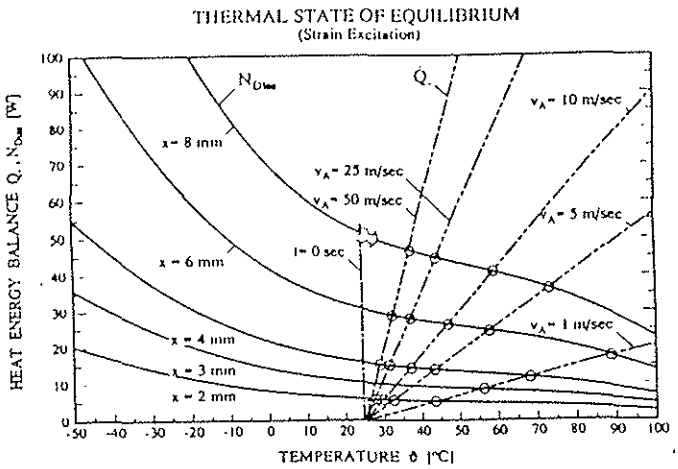

Fig. 26 : Thermal equilibrium state at strain excitations.

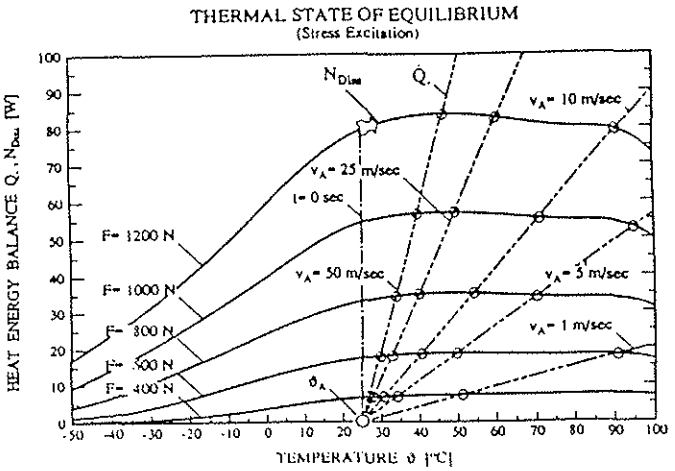

Fig. 27 : Thermal equilibrium state at stress excitations.

The effect of ambient temperature ϑ_A and cooling velocity v_A on stiffness K' ,dissipation power N_{Diss} and average damper temperature ϑ is explicitly shown in Figures 28 to 30 (strain excitation) and Figures 31 to 33 (stress excitation) .

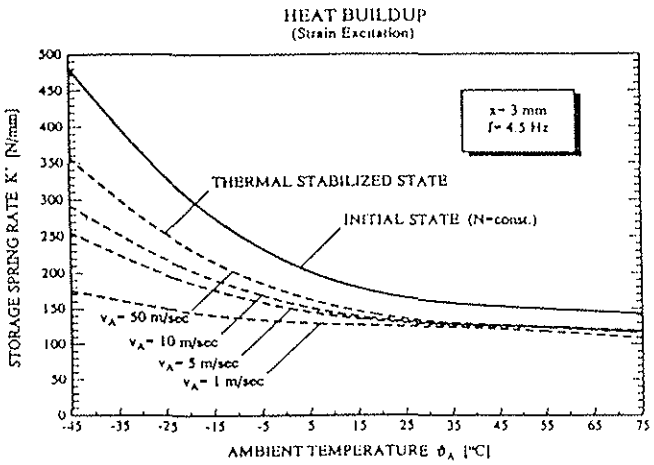

Fig. 28 : Storage spring rate K' versus ambient temperature and airflow velocity (strain excitation) .

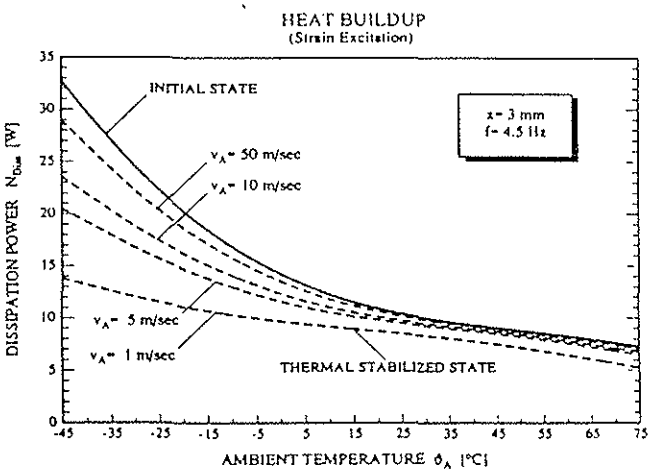

Fig. 29 : Dissipation power N_{Diss} versus ambient temperature and airflow velocity. (strain excitation) .

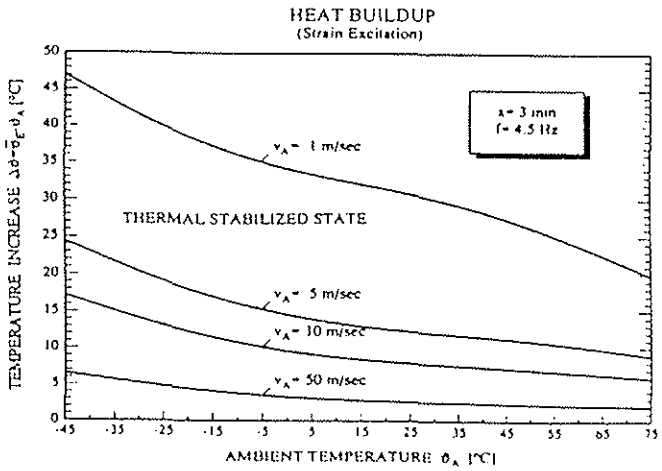

Fig. 30 : Temperature increase $\Delta\vartheta$ versus ambient temperature and airflow velocity (strain excitation) .

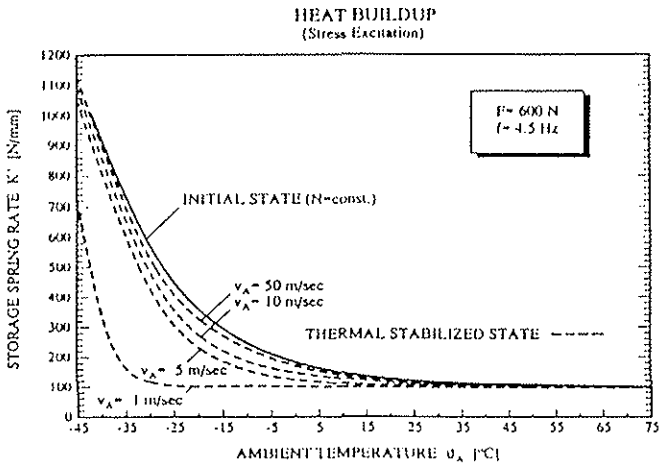

Fig. 31 : Storage spring rate K' versus ambient temperature and airflow velocity (stress excitation) .

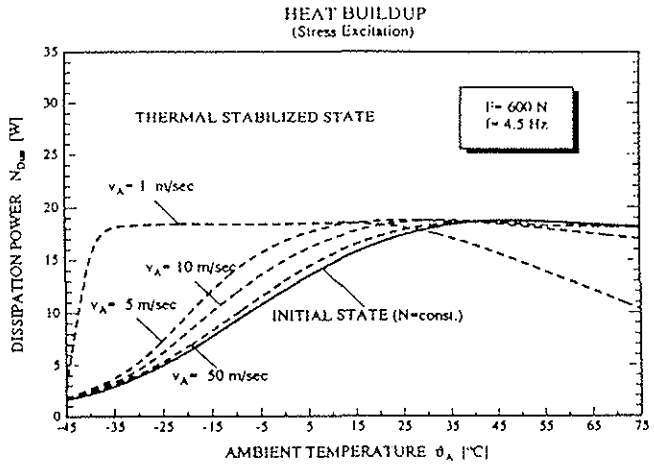

Fig. 32 : Dissipation power N_{Diss} versus ambient temperature and airflow velocity. (stress excitation) .

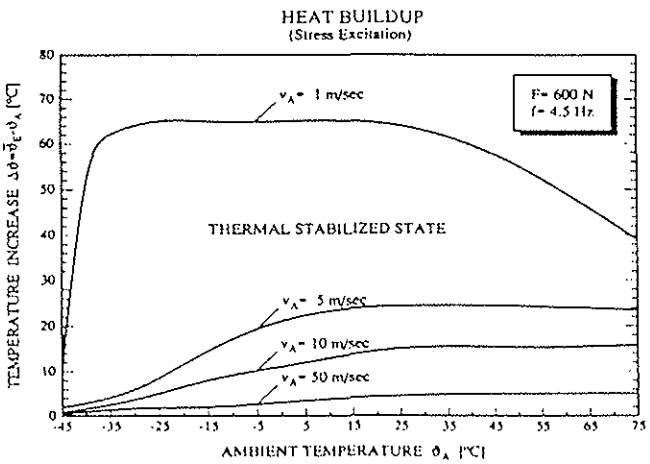

Fig. 33 : Temperature increase $\Delta\vartheta$ versus ambient temperature and airflow velocity (stress excitation) .

All these examples demonstrate the significant effect of ambient temperature ,cooling intensity and selfheating on the damper characteristic . As a further result ,the calculated dissipation energy N_{Diss} can be used in combination with an FEM analysis for the calculation of temperature distribution and therefore peak temperatures within the elastomer.

2.6 Application to Rotor Blade Lead-Lag Damping

One important application of the discrete damper model is the analytical prediction of the modal lead-lag damping ratio D_ζ and the first lead-lag eigenfrequency ω_ζ under consideration of damper nonlinearities.
A simplified numerical model for rotor blade damping with an integrated discrete damper model is shown schematically in Figure 34 .
The stepwise iterative solution of this coupled nonlinear system for steady state operating conditions yields the modal lead-lag damping and frequency ratio versus lead-lag amplitude in dependency of the damper temperature. The example in Figure 35 shows the amplitude effect of the modal lead-lag damping and the corresponding lead-lag frequency ratio at different temperatures . Other sources of rotor damping,such as structural resp. aeroelastic damping are not considered here.

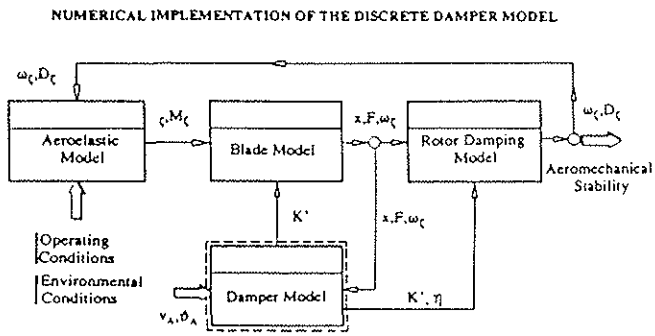

Fig. 34 : Simplified quasi- steady state model for the prediction of the modal rotor blade damping capacity.

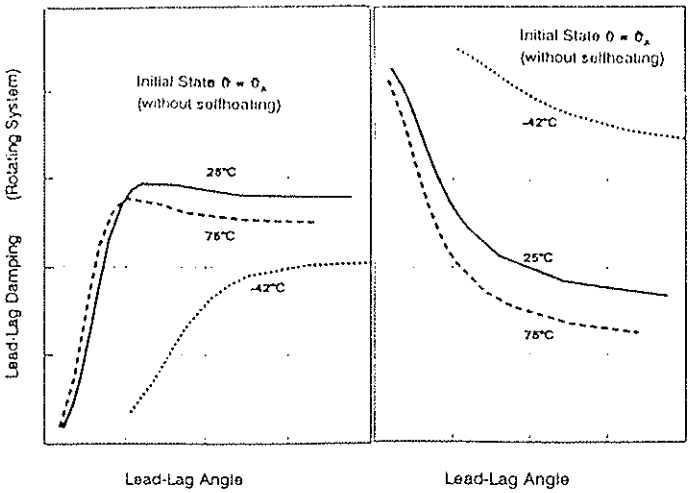

Fig.35 : Rotor blade lead-lag damping and lead-lag frequency in dependency of lead-lag angle and temperature.

3. Thermomechanical Damper Model with Distributed Parameters

3.1 Basic Considerations to the FEM in the Nonlinear Viscoelasticity

The description of the elastomeric damper with distributed parameters (stress, strain, temperature, heat transfer, etc.) leads to a coupled thermo - viscoelastic finite element analysis.
A frequency domain analysis with nonlinear FEM codes / 6 / is usually limited to small-amplitude vibrations of thermorheologically simple visco - elastic solids. This method neglects the effect of the load amplitude on spring rate and loss factor /6/
A time-domain analysis of the thermoviscoelastic damper model for arbitrary periodic loads is usually separated in two basic steps:

- Numerical integration over a cycle of deformation for the calculation of the nonlinear visco-elastic response and the corresponding dissipation energy.Temperature changes during this load cycle are neglected.

- Calculation of the transient temperature field with a temperature dependent " cycle - averaged " heat source .

The first step yields an inhomogeneous distribution of the dissipative heat source as well as a global mean value at different temperature boundary conditions.
A complete coupled thermoviscoelastic analysis for the transient thermal state is too expensive in the design stage and must be limited to selected, critical load cases. In addition, thermorheologically complex material behaviour and a different amplitude dependency for the equilibrium and hereditary term of the viscoelastic constitutive equation are not realized today in finite element modules for nonlinear-viscoelastic problems.
In this paper the application of the FEM method was restricted to a steady state heat transfer analysis with temperature dependent source terms by the concentrated parameter model.

3.2 FEM calculation of the temperature distribution within the damper

The basic equation which covers the most heat transfer analysis problems is the partial Fourier differential equation

$$\frac{\partial \vartheta}{\partial t} = \frac{\lambda}{c \cdot \rho} \cdot \left(\frac{\partial^2 \vartheta}{\partial x^2} + \frac{\partial^2 \vartheta}{\partial y^2} + \frac{\partial^2 \vartheta}{\partial z^2} \right) + \frac{n_{Diss}}{c \cdot \rho}$$

which relates the temperature change by time to the temperature distribution in space.
The parameter λ is the coefficient of thermal conductivity, c is the specific heat capacity and ρ is the density . n_{diss} represents the dissipation energy per unit volume ,which can be regarded as an internal distributed heat source produced by cyclic damper deflections.
In order to solve the Fourier equation the thermal boundary conditions must be defined.
During operation the damper is blown by air and an exchange of heat occurs.
The specific heat flow from the surface of the damper to the surrounding air flow is given by the expression

$$\dot{q}_i = \alpha_i (\vartheta_W - \vartheta_A)$$

with the coefficient of heat conduction α_i (index i means the surface i ,where heat conduction takes place), the surface temperature ϑ_W and the temperature ϑ_A of the surrounding air flow.
The corresponding α -values can be calculated for free and forced convection according to Ref. / 1,2 /, or are estimated by experiments. In the first step it can be assumed,that the α - values are identical at all points of the outer damper surface .
Together with the initial temperature

$$\vartheta(t=0) = \vartheta_0$$

all required boundary conditions of the heat transfer problem are known .
The Finite Elemente Program MARC (Ref. / 6 /) was used here for the solution of this parabolic differential equation.
The element library of MARC contains an 8 - node axisymmetric isoparametric quadrilateral element which was used for the calculations.

Using the FEM method the solution of the Fourier equation reduces to solve the matrix equation for the whole temperature field :

$$\mathbf{C}\,(d\vartheta/dt) + \mathbf{K}\,\vartheta = \mathbf{Q}$$

The vectors ϑ and $d\vartheta/dt$ are the nodal temp - eratures at time t and its time derivatives .
C and **K** are the matrix of heat capacity and the heat transfer matrix.
Q is defined as the heat flow vector at the nodal points.
For the steady state case the time derivative of the temperature $d\vartheta/dt = 0$ and the corresponding matrix equation reads :

$$\mathbf{K}\,\vartheta = \mathbf{Q}$$

The solution vector for the temperature ϑ turns then out to be

$$\vartheta = \mathbf{K}^{-1}\,\mathbf{Q}$$

Examples :

In order to investigate the peak temperatures and the influence of the metal shims on temperature distribution,two different FEM calculations for a lead-lag damper with and without metal shims have been carried out for the steady state case.
The coefficients of heat conduction α_i are calculated according to Ref. /1 , 2 / for forced and free convection assuming an air flow velocity of about w_A = 50 m/sec , see also Figure 24.

The dissipative energy N_{Diss} of the global damper model was calculated for given boundary conditions and dynamic loads using the concen - trated parameter model.
For the FEM calculation of peak temperature within the damper an homogeneous distribution of the dissipated energy

$$n_{Diss} = N_{Diss} / V_E \neq f(x)$$

is assumed . Figures 36 to 37 show the calculated temperature distributions within the damper.

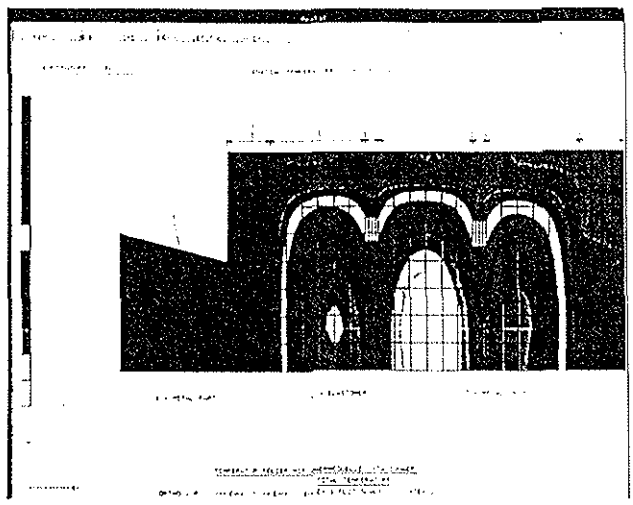

Fig. 36 : Temperature distribution within a damper with metal shims.

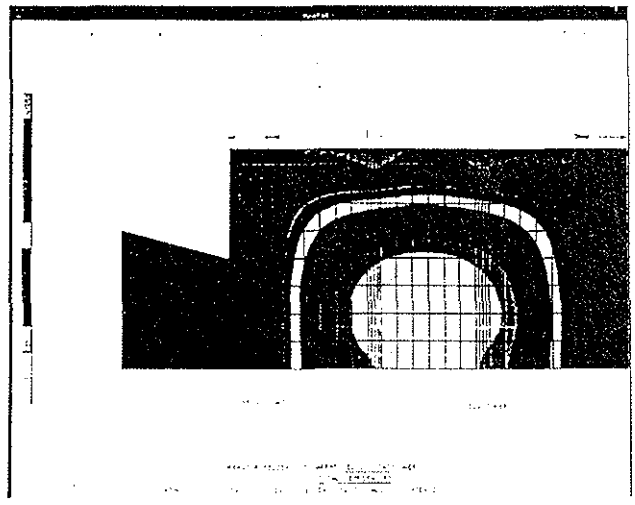

Fig. 37 : Temperature distribution within a damper without metal shims.

Due to the cooling effect of the two metal shims, the maximum temperature for the first example was found to be :

$$\vartheta_{max} = 31\ C°$$

Without metal shims, the peak temperature is higher and turns out to be :

$$\vartheta_{max} = 43\ C°$$

Taking into account an initial temperature of

$$\vartheta_0 = 20\ C°$$

the relationship between peak temperature ϑ_{max}

and the integral mean temperature $\vartheta = \overline{\vartheta}$ (concentrated parameter model) was found to be

$$\beta_\vartheta = \vartheta_{max}/\vartheta = 31\ C°/25.25C° = 1.23$$
(damper with shims)

respectively

$$\beta_\vartheta = \vartheta_{max}/\vartheta = 43\ C°/25.78C° = 1.67$$
(damper without shims)

Summary

An engineering model for the prediction of the thermoviscoelastic response of discrete elastomeric lead-lag dampers under cyclic loading was developed. This model is based on amplitude dependent complex moduli and involves material nonlinearities and nonlinearity effects due to thermomechanical coupling.
Numerical studies were carried out with this concentrated parameter model with intent to investigate the influence of load amplitude, frequency,ambient temperature and cooling rate on the heat build up and damper properties.
Criteria for thermal overheating were derived and the effect of polyharmonic excitations on self - heating was considered.
The difference in the thermoviscoelastic response with respect to displacement and force controlled cyclic excitations was discussed and the application of this concentrated parameter model for the prediction of rotor blade damping was demonstrated.
In addition a finite element analysis was carried out for the determination of the peak temperatures within the elastomer.
Finally,a brief outline was given to damper models with distributed parameters.
In conclusion,this engineering model shows a simple way to simulate the effects of thermo - mechanical coupling and nonlinearities on the dynamic properties of elastomeric dampers , mastering the loadcase temperature.
The reported results cover the first stage of theoretical and experimental investigations concerning the thermomechanical design of dampers. Further activities in the analytical damper characterization are the time domain formulation for arbitrary loads and its numerical realization such as the experimental verification of the temperature effect during flight tests.

References

/1/ Wong, H.Y., "Heat Transfer for Engineers", Longman Group Ltd., London, 1977

/2/ VDI-Wärmeatlas, 6. Auflage, 1988, Berechnungsblätter für den Wärmeübergang, VDI-Verlag, Düsseldorf

/3/ Schillinger, A., "Internal Test Reports", ECD, Ottobrunn,Germany, 1986-1992

/4/ Schwarzl, F.R., "Polymermechanik", Springer-Verlag, Berlin, 1990

/5/ Ferry, J.D., "Viscoelastic Properties of Polymers", John Wiley & Sons, New York, 1980

/6/ MARC Program Documentation, Volume A to F, Revision K.4, January 1990, MARC Analysis Research Corporation, Palo Alto, CA, USA

/7/ Constable, I., Williams, J.G. and Burns, D.J., "Fatigue and Cyclic Thermal Softening of Thermoplastics, Journal of Mech. Eng. Science, Vol.12, No.1, 1970

/8/ Press, W.H., Flannery, B.P., Tenkolsky, S.A. and Vetterling, W.T., "Numerical Recipes (FORTRAN Version)", Cambridge University Press, Cambridge, 1989

/9/ Lazan, B.J., "Damping of Materials and Members in Structural Mechanics", Pergamon Press, Oxford, 1968

/10/ Schimke, D., Enenkl, B., Allramseder, E., "MBB BO 108 Helicopter Ground and Flight Tests Evaluation", Proceedings of the 15th EUROPEAN ROTORCRAFT FORUM, September 1989, Amsterdam

/11/ Tauchert, T.R., "Transient Temperature Distributions in Viscoelastic Solids Subject to Cyclic Deformations", Acta Mechanica 6, 239-252, 1968

/12/ Felker, F.F., Lau, B.H., McLaughlin, S.M. and Johnson, W., "Nonlinear Behaviour of an Elastomeric Lag Damper Undergoing Dual-Frequency Motion and its Effect on Rotor Dynamics", Journal of AHS, October 1987

/13/ Hausmann, G., "Structural Analysis and Design Considerations of Elastomeric Dampers with Viscoelastic Material Behaviour" Proceedings of the 12th EUROPEAN ROTORCRAFT FORUM, September 1986, Garmisch-Partenkirchen

/14/ Brüller, O.(ed.), "Applied Viscoelasticity of Polymers", CISM, Udine, July 3-7, 1989

/15/ Ottl , D. "Nichtlineare Dämpfung in Raum - fahrtstrukturen " , VDI-Fortschrittsbericht Reihe 11,Nr. 73,VDI-Verlag,Düsseldorf,1985

/16/ Fesko,D.G.,Tschoegl,N.W., "Time-Temperature Superposition in Thermorheologically Complex Materials",J.Polym.Science:Part C, No. 35, pp. 51- 69 ,1971

/17/ Ridell,M.N.,Koo G.P. O'Toole,J.L. "Fatigue Mechanisms of Thermoplastics" , Polymer Engineering and Science , October 1966

/18/ Parker,N.S. and Hilbert,G.E. " The Interpre - tation of dynamic measurements of non - linear viscoelastic materials " , Rheologica Acta, 1974,13,N° 6 , pp. 910-915

/19/ Fletcher,R.: "Practical Methods of Opti - mization " ,Vol. I to II , John Wiley,Chichester 1980/1981